ORIJINAL MƏQALƏ **AÇIQ GİRİŞ (OPEN ACCESS)**

IN VİTRO ASSESSMENT OF BİOACTİVE MOLECULE-LOADED 3D-PRİNTED CHİTOSAN/MAGNESİUM-DOPED HYDROXYAPATİTE SCAFFOLDS FOR BONE TİSSUE REGENERATİON

Hefzollesan Sahar[1,2*], Musayeva H.[1], Mammadov A.[1] , Hefzollesan Sahra [3], Mammadov R.[1]

Abstract

The development of bioactive and biodegradable scaffolds through three-dimensional (3D) printing has emerged as a promising strategy for bone tissue engineering. In this study, a 3D-printed composite scaffold based on chitosan and magnesium-doped hydroxyapatite (Mg-HAp) functionalized with bioactive molecules including icariin, lithium chloride, and naringin was successfully fabricated and evaluated through in vitro investigations. Magnesium-doped hydroxyapatite nanoparticles were synthesized using a sol–gel method and incorporated into a chitosan matrix to produce a printable composite ink. The scaffolds were fabricated using extrusion-based 3D printing and subsequently freeze-dried to obtain a porous architecture suitable for cellular interaction. Physicochemical characterization of the scaffolds was performed using Fourier transform infrared spectroscopy (FTIR) and scanning electron microscopy (SEM), confirming the successful integration of polymeric and ceramic components. The scaffolds exhibited an interconnected porous structure with favorable pore size distribution and high swelling capacity, indicating their suitability for nutrient diffusion and cell attachment. Bioactivity evaluation in simulated body fluid demonstrated the formation of apatite-like mineral layers on the scaffold surface, confirming their biomineralization capability.

Biological performance was assessed using MC3T3-E1 osteoblast-like cells. Cell viability analysis using the CCK-8 assay showed enhanced cell proliferation after 24 and 72 h, indicating good cytocompatibility. SEM observations confirmed effective cell attachment and spreading on the scaffold surface. Furthermore, gene expression analysis using RT-qPCR demonstrated significant upregulation of the Wnt/β-catenin signaling pathway, suggesting that the incorporated bioactive molecules promote osteogenic differentiation. Overall, the results indicate that the developed 3D-printed chitosan/Mg-HAp scaffold loaded with icariin, lithium chloride, and naringin exhibits favorable physicochemical properties, cytocompatibility, and osteogenic potential in vitro. These findings highlight the potential of the proposed scaffold system as a promising candidate for bone tissue engineering applications.

Keywords: 3D Printing, Tissue Engineering. Icariin, Mg-HAP, Naringin, Chitosan,Bone Density.

INTRODUCTİON

Tissue engineering has emerged as an alternative strategy focused on designing and constructing scaffolds and biomimetic biomaterials to repair tissue structures and positively interact with biological systems to initiate regeneration [1,2]. It integrates concepts from materials science, cell biology, and immunology, offering multifunctional therapeutic tools. Scaffolds are particularly promising because they mimic the natural extracellular matrix,

providing an ideal biological environment for cell adhesion, proliferation, differentiation, and migration, which are essential for effective bone regeneration [1,3]. Additionally, the development of bioactive and biocompatible materials helps regulate the immunological environment, promoting healing and controlling chronic inflammation in bone tissue [3]. The bone matrix itself consists of mineral and organic components that are highly compatible and suitable for such applications [4-9].

One of the widely used polymers in tissue engineering is chitosan, known for its biocompatibility, antibacterial properties, and ability to support wound healing and tissue repair. Its non-toxicity and capacity to stimulate the immune system make it highly valuable in biomedical applications. Furthermore, chitosan is biodegradable, allowing it to be naturally absorbed in the body, which is crucial for medical use [10,11]. Studies such as Wang et al. (2017) have demonstrated that incorporating lipid derivative-based extracellular matrix components into chitosan enhances the recruitment and proliferation of bone marrow mesenchymal cells. Chitosan also improves the mechanical strength and bioactivity of scaffolds, increasing their osteogenic potential [12]. Its combination with hydroxyapatite in nanocomposites has been extensively studied to match the mechanical properties of human bone tissues [13-16].

Hydroxyapatite (HAP), a ceramic nanocomposite, is another important material in tissue engineering because it closely resembles the mineral component of bone. It exhibits excellent biocompatibility and supports bone regeneration, making it widely applicable in medicine and dentistry [17,18]. However, its major limitation is poor mechanical strength [19,20]. To address this issue, researchers have explored the incorporation of metal ions to enhance both mechanical and biological properties. Magnesium (Mg), in particular, has shown promising results due to its fracture toughness and Young's modulus, which are similar to those of natural bone [21]. Magnesium also plays a crucial role in bone metabolism and can enhance bone formation when incorporated into scaffolds [22].

Nanocomposites composed of polymers and ceramics have demonstrated effectiveness in mimicking the nanoscale structure and biological properties of bone. In this study, chitosan–magnesium–hydroxyapatite nanocomposites were combined with bioactive agents such as icariin, lithium chloride, and naringin. Icariin, derived from Epimedium species, promotes osteogenesis through the BMP-2/RUNX2 signaling pathway and enhances osteoblast growth and mineralization [23-25]. Lithium chloride acts as an activator of the Wnt/β-catenin pathway, which regulates cellular growth, proliferation, and differentiation, and supports angiogenesis and tissue regeneration [26-28]. Naringin, a flavonoid from citrus fruits, exhibits anti-inflammatory and angiogenic properties and promotes bone formation by increasing BMP-2 expression [29-32]. These bioactive

Yazışma üçün əlaqə:
Hefzollesan Sahar[1,2*], Musayeva H.[1], Mammadov A.[1], Hefzollesan Sahra [3], Mammadov R.[1]
1 Azerbaijan Medical University, Department of Therapeutic Dentistry and Prosthodontics, Baku
2 MedEra Hospital, Dental Department, Baku, Azerbaijan
3 Karadeniz Technical University, Department of Dentistry, Trabzon, Turkey
*E-mail: sahar.hefzollesan@amu.edu.az

compounds can be used individually or synergistically to enhance osteogenic activity and bone regeneration.

Recent advancements in three-dimensional (3D) printing technology have significantly improved scaffold design in tissue engineering. This technology allows precise control over scaffold architecture, including surface roughness, fiber arrangement, and pore structure. Such control enables the creation of complex scaffolds that closely resemble natural bone, thereby promoting cell growth and differentiation. 3D printing is increasingly used in bone repair and regeneration, particularly in cases where natural healing is insufficient, such as severe injuries or large bone defects [33-36].

The primary aim of this study is to develop scaffolds capable of healing critical-sized bone defects and enhancing osteogenesis in patients with compromised healing, such as those with osteoporosis or severe fractures, where natural bone repair is limited due to age, trauma, or surgical resection [37]. Although chitosan and hydroxyapatite are commonly used, the integration of magnesium doping along with a multifunctional bioactive cocktail (icariin, lithium chloride, and naringin) within 3D-printed scaffolds is novel.

This study proposes a unique nanocomposite scaffold that combines these materials to regulate the Wnt/β-catenin signaling pathway. The scaffold is designed as a dual-function system that mimics the mineral composition of bone while simultaneously promoting osteogenesis and angiogenesis through bioactive molecules. Chitosan provides a biodegradable and antibacterial structural matrix, magnesium/doped hydroxyapatite (Mg-HAp) enhances osteoconductivity and mechanical strength, and the bioactive cocktail stimulates key signaling pathways involved in bone regeneration.

Based on this concept, the study hypothesizes that incorporating this bioactive cocktail into an extrusion-based 3D-printed scaffold can create a synergistic microenvironment. This environment is expected to provide mechanical stability while activating multiple osteogenic pathways, thereby significantly improving bone regeneration compared to conventional scaffolds. The main objective is to develop this novel scaffold and evaluate its mechanical properties, biocompatibility, and osteogenic potential through both in vitro and in vivo studies.

MATERİALS AND METHODS

Preparation of Chitosan Solution

Chitosan powder (degree of deacetylation ≥75%, medium molecular weight) was purchased from Sigma-Aldrich (USA). Calcium nitrate tetrahydrate, magnesium nitrate hexahydrate, and ammonium dihydrogen phosphate used for hydroxyapatite synthesis were obtained from Merck (Germany). Icariin, lithium chloride, and naringin were also supplied by Sigma-Aldrich. All other chemicals, including glacial acetic acid, were of analytical grade.To prepare the chitosan solution, 0.2 g of chitosan was dissolved in 50 mL of 2% acetic acid and stirred for 6 h at room temperature until a homogeneous solution was obtained.

Synthesis of Magnesium-Doped Hydroxyapatite (Mg-HAp)

Magnesium-doped hydroxyapatite nanoparticles were synthesized using a sol–gel process. Calcium nitrate and magnesium nitrate were mixed at different Mg/Ca molar ratios (0:1, 0.1:0.3, and 0.1:0.5) and stirred for 1 h to form a uniform precursor solution. Ammonium dihydrogen phosphate was then slowly introduced

under continuous stirring to initiate gel formation.

The resulting white gel was aged at room temperature for 24 h and subsequently calcined at 600 °C for 2 h. After calcination, the material was ground to obtain fine Mg-HAp nanopowder, which was later used in the fabrication of nanocomposite scaffolds.

Fabrication of 3D Printing Scaffold

A chitosan solution was prepared by dissolving chitosan in 2% (v/v) acetic acid to obtain a concentration of 4.5% (w/v), followed by continuous stirring at room temperature for 6 h until a homogeneous solution was formed. Magnesium-doped hydroxyapatite (Mg-HAp) was then incorporated into the chitosan solution at a concentration of 0.45% (w/v) and mixed manually for 1 h to ensure uniform dispersion.

Subsequently, bioactive molecules including icariin (0.5 mg/mL), lithium chloride (1 mM), and naringin (0.1 mg/mL) were added to the chitosan/Mg-HAp mixture and stirred for an additional 1 h to obtain a homogeneous composite ink.

The scaffold structures (20 mm×20 mm×2 mm lattice design) were modeled using CATIA V5 developed by Dassault Systèmes (Vélizy-Villacoublay, France). The scaffolds were then fabricated using an extrusion-based 3D printing technique with the Abtin II 3D Printer manufactured by Abtin Fanavar (Iran).

After printing, potassium hydroxide (KOH) supplied by Merck was gradually added to the scaffolds for neutralization. After 10 min, the scaffolds were collected and stored at −20 °C. Freeze-drying was subsequently carried out after 24 h at 55 °C and 0.040 bar using an Alpha 1-2 LD plus freeze dryer manufactured by Martin Christ Gefriertrocknungsanlagen GmbH (Germany).

Characteristics of 3D Printed Scaffolds

Fourier Transform Infrared Spectroscopy (FTIR)

Fourier transform infrared spectroscopy (FTIR) was used to identify the functional groups and interactions between the polymeric and ceramic components of the composite scaffolds. The analysis was performed using the Tensor 27 FTIR Spectrometer manufactured by Bruker. The samples were ground with potassium bromide (KBr) to prepare pellets prior to analysis. FTIR spectra were recorded within the wavenumber range of 500–4000 cm^{-1}.

Porosity and Pore Size Measurement

The porosity and pore size distribution of the fabricated scaffolds were evaluated using scanning electron microscopy (SEM) images. The obtained images were analyzed using ImageJ (version 1.48v, USA). Porosity was calculated as the ratio of pore area to the total surface area of the scaffold image. Multiple SEM images were analyzed, and the average values were reported.

Swelling Behavior of Scaffolds

The swelling behavior of the scaffolds was investigated by immersing the samples in phosphate-buffered saline (PBS). Prior to the experiment, scaffold samples (10 mm × 10 mm × 2 mm) were freeze-dried and weighed to obtain the initial dry weight (Wd). The samples were then incubated in PBS solution (pH 7.4) at 37 °C.

At predetermined time intervals, the scaffolds were removed from the solution, and excess surface liquid was carefully removed using filter paper. The swollen scaffolds were then weighed to determine the wet weight (Ww). The swelling ratio was calculated using the following equation:

$$\text{Swelling Ratio (\%)} = (Ww - Wd) / Wd \times 100$$

Where W_w represents the wet weight of the sample and W_d represents the initial dry weight.

Scaffold Bioactivity

The in vitro bioactivity of the fabricated scaffolds was evaluated by immersing them in simulated body fluid (SBF, 1× concentration). Scaffold samples with predetermined dimensions were prepared, and the required volume of SBF was calculated using the equation:

$V = S / 10$

V = required volume of simulated body fluid (SBF) in **mL**

S = surface area of the scaffold in **mm²**

Mechanical Compression Test

The compressive mechanical properties of the scaffolds were determined using the AG-X Plus Universal Testing Machine manufactured by Shimadzu. Scaffold samples were prepared with dimensions of 10 × 10 × 5 mm³. Compression testing was performed between two steel plates at a constant crosshead speed of 1 mm/min until deformation occurred.

In Vitro Biological Assay

Cell Culture

Osteoblast-like cells (MC3T3-E1, NCBI C555) obtained from the Pasteur Institute of Iran were used for the in vitro biological experiments. The cells were cultured in Dulbecco's Modified Eagle's Medium/Nutrient Mixture F-12 (DMEM/F-12) supplemented with fetal bovine serum (10%) and penicillin–streptomycin (1%). The cultures were maintained at 37 °C in a humidified incubator containing 5% CO_2.

Cell Morphology Assessment

To evaluate cell morphology on the scaffolds, approximately 2 × 10⁴ MC3T3-E1 cells were seeded onto each scaffold in DMEM/F-12 medium supplemented with 10% fetal bovine serum. After 24 h of incubation, the scaffold–cell constructs were removed from the culture medium and gently washed with phosphate-buffered saline (PBS).

The samples were then fixed with 2.5% glutaraldehyde supplied by Sigma-Aldrich for 2 h. Following fixation, the constructs were dehydrated through a graded ethanol series, dried, and sputter-coated with gold. The morphology and attachment of the cells on the scaffold surface were subsequently examined using scanning electron microscopy (SEM).

Cell Viability Measurement on Scaffolds

Cell viability and proliferation were evaluated using a Cell Counting Kit-8 (CCK-8) assay. Two experimental groups were considered:

1. **Experimental group** ; MC3T3-E1 cells cultured on the fabricated nanocomposite scaffolds.
2. **Control group (positive control)** ; MC3T3-E1 cells cultured directly on tissue culture polystyrene (TCP) plates without scaffolds.

Prior to cell seeding, scaffold samples (6 mm diameter, 2 mm thickness) were sterilized with 70% ethanol and ultraviolet irradiation for 2 h, followed by washing with PBS. Cells were seeded onto both scaffold and control wells at a density of 5 × 10³ cells per well.

After incubation periods of 24 and 72 h, 10 µL of CCK-8 reagent was added to each well and the plates were further incubated at 37 °C. The optical density (OD) was then measured at 450 nm using a microplate spectrophotometer to determine cell metabolic activity.

Determination of Minimum Inhibitory Concentration (MIC)

The antibacterial activity of the scaffolds was evaluated by determining the minimum inhibitory concentration (MIC) against Staphylococcus aureus using the broth microdilution method according to the

guidelines of the Clinical and Laboratory Standards Institute.

An overnight culture of *S. aureus* was prepared and adjusted to a turbidity equivalent to the 0.5 McFarland standard (approximately 1.5×10^8 CFU/mL) using a spectrophotometer at 625 nm. Scaffold suspensions were serially diluted in nutrient broth to obtain concentrations ranging from 1 to 1024 µg/mL in a 96-well microplate.

Subsequently, 100 µL of the bacterial suspension was added to each well containing the scaffold dilutions. For assay validation, two control groups were included:

- **Positive control:** bacterial suspension with nutrient broth without scaffold material to confirm bacterial growth.
- **Negative control:** sterile broth without bacteria to ensure medium sterility.

The microplates were incubated at 37 °C for 24 h. The MIC value was defined as the lowest scaffold concentration that completely inhibited visible bacterial growth.

RT-qPCR Analysis of Wnt/β-Catenin Gene Expression

Quantitative real-time PCR (RT-qPCR) was performed to evaluate the expression levels of the Wnt and β-catenin genes in MC3T3-E1 cells cultured on the scaffolds. Cells grown on tissue culture polystyrene (TCP) plates served as the control group.

Total RNA was extracted from both experimental and control samples using TRIzol reagent supplied by DNAbiotech, ensuring identical processing conditions for all samples. The extracted RNA was subsequently reverse-transcribed into complementary DNA (cDNA) using the SuperRT cDNA synthesis kit (DNAbiotech) according to the manufacturer's instructions.

Quantitative PCR analysis was performed using Ultra SYBR mix provided by DNAbiotech. The primer sequences for the target genes (Wnt and β-catenin) as well as the housekeeping gene GAPDH are listed in Table 1. Gene expression levels were calculated using a comparative method, where the expression of the target genes was normalized to GAPDH and expressed as fold changes relative to the control group.

Table 1. Sequences of primers for the expression of Wnt/β-catenin genes and the reference gene GAPDH

Gene	Sequencing Primers
Wnt	F: TCTTACACGACCCAAAGCCC
	R: CAAGTCACCGTCCCTCCAAA
GAPDH	F: AGGTCGGTGTGAACGGATTTG
	R: TGTAGACCATGTAGTTGAGGTCA
β-catenin	F: CCTACACAACCTTTCCCACCA
	R: CTGGCGACCCAAGCATTTTC

RESULTS

Structural Characterization of the Fabricated Composite Scaffold

Fourier transform infrared spectroscopy (FTIR) analysis was performed to identify the functional groups of the individual components and to investigate the chemical interactions within the composite scaffold. The spectra of pure chitosan, synthesized magnesium-doped hydroxyapatite (Mg-HAp), and the fabricated 3D-printed nanocomposite scaffold were compared to confirm the successful incorporation of the ceramic phase into the polymer matrix. The corresponding FTIR spectra of chitosan, Mg-HAp, and the composite scaffold are presented in Figure 1.

Typical bands with chitosan at the purity spectrum (1650 cm^{-1}, Amide I, C=Ostretching) and (1590 cm^{-1}, Amide II, N-H bending) were recorded. The wide band in the area of 3000–3500 cm^{-1} is related to overlapping O-H and N-H vibrations. In the Mg-HAp sample, the characteristic phosphate group () bands were observed at 1030 cm^{-1} and 603 cm^{-1}, as well as OH^- vibrations at 3570 cm^{-1}.

The spectrum of the final nanocomposite scaffold combined characteristic peaks of the polymer matrix and ceramic filler, confirming successful incorporation. Notable spectral changes were observed: the amide I band at 1650 cm^{-1} shifted, and the asymmetric COO^- absorption at 1450 cm^{-1} became more pronounced, indicating interaction between the ceramic phase and the functional groups of chitosan. The intensity of the broad band at 3000–3500 cm^{-1} also increased, reflecting enhanced hydrogen bonding among the scaffold components and the loaded bioactive agents (icariin, lithium chloride, and naringin). These spectral changes confirm the formation of a stable composite structure suitable for bone tissue engineering.

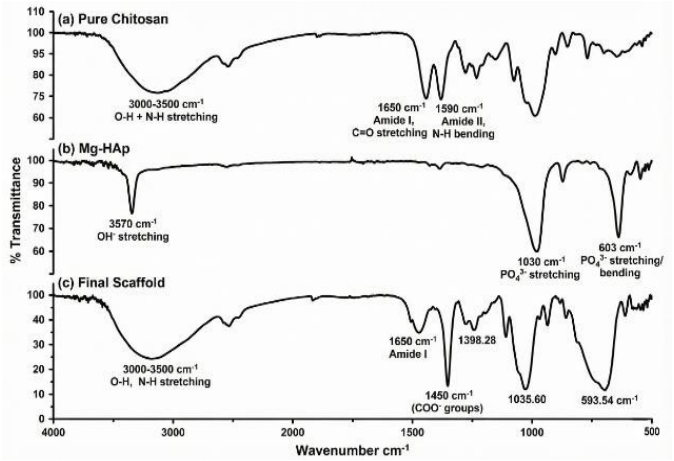

Figure 1. FTIR spectrums of pure Chitosan, synthesized Magnesium-doped Hydroxyapatite (Mg-HAp), and the final 3D printed nanocomposite scaffold doped with bioactive agents, are compared, and confirm successful incorporation of components.

SEM images of 3D Scaffolds and Porosity and Pore Size of Scaffolds

The blank scaffolds with an average thickness of 451 μm showed chitosan and hydroxyapatite fibers, doped with magnesium and loaded with bioactive components (icariin, lithium chloride, and naringin), with an average length of 56μm. Therefore, the average pore size of the scaffolds was higher (879 μm). The

scaffolds had visible micropores, the diameter of which is less than 10 μm. The scaffolds are therefore porous in nature with well-defined pores and strong pore walls. The lyophilization process had no effect and did not cause any shrinkage or other tissue anomalies.

Figure 2 shows SEM images of 3D scaffolds at a higher viewing angle. Table 2 is a summary of fiber thickness, pore size, percentage of porosity, and degree of porosity.

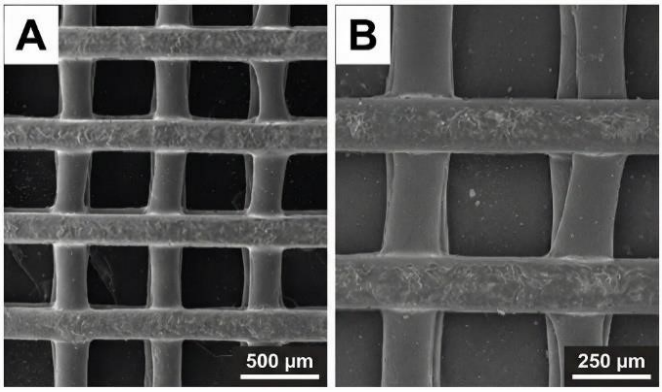

Figure 2. Scanning Electron Microscopy (SEM) micrographs of the 3D printed nanocomposite scaffolds showing the structural morphology.(A).low magnification view of the lattice structure illustrating interconnected pores (Scale bar: 500 μm).(B). High magnification view detailing the surface roughness and fiber integrity (Scale bar: 250 μm).

Table 2. Dimensions of 3D printed scaffolds

	3D printing scaffold
(μm) Strand thickness	451±23
(μm) Pore size	879±12
Porosity percentage	85.17±4.1

Swelling Behavior of the Scaffolds

The swelling properties of the scaffolds were evaluated by monitoring their water absorption capacity (Figure 3). The results demonstrated that the dry scaffolds were capable of absorbing a considerable amount of water, indicating a high swelling capacity. As the immersion time increased, the swelling ratio gradually increased due to continuous water uptake by the scaffold structure.

However, after prolonged immersion, the rate of water absorption decreased and the scaffolds eventually reached a swelling equilibrium. The highest swelling ratio was observed in the chitosan/Mg-HAp scaffolds containing the bioactive compounds icariin, lithium chloride, and naringin.

Furthermore, the results indicated that the addition of these bioactive molecules did not significantly alter the overall swelling kinetics of the scaffold. The observed swelling behavior can be attributed to the hydrophilic nature of the chitosan matrix and the porous architecture of the scaffol

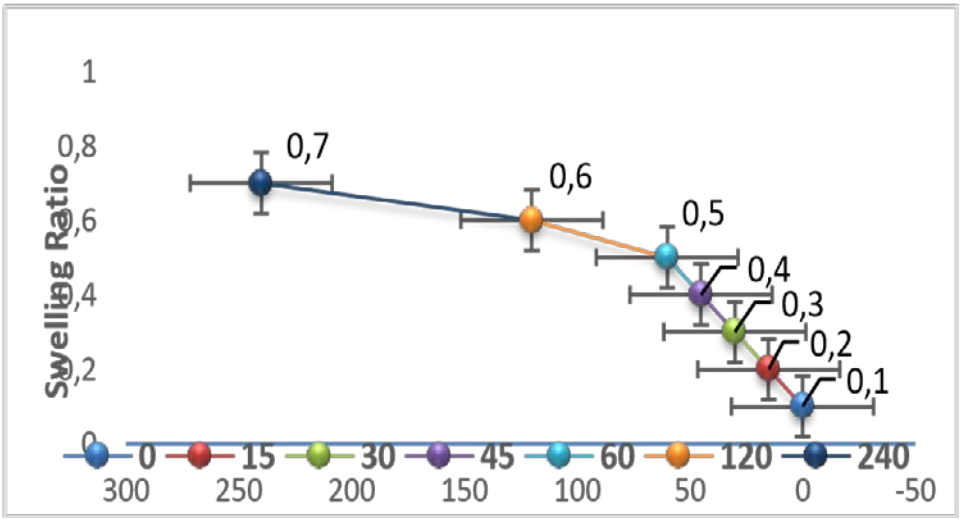

Figure 3. Swelling ratio of printed scaffold

Bioactivity of the Scaffolds

The bioactivity of the scaffolds was assessed by evaluating biomineralization after immersion in simulated body fluid (SBF) for 30 days. SEM analysis revealed the formation of dense, globular apatite-like mineral deposits covering the surface of the scaffold fibers (Figure 4).

To further confirm the chemical composition of the deposited mineral layer, Energy Dispersive X-ray Spectroscopy (EDS) analysis was performed. The EDS spectra showed strong signals corresponding to calcium (Ca) and phosphorus (P), indicating the formation of calcium phosphate phases on the scaffold surface. These findings confirm the excellent biomineralization ability of the composite scaffold and demonstrate its potential to promote bone-like apatite formation, which is essential for bone tissue regeneration.

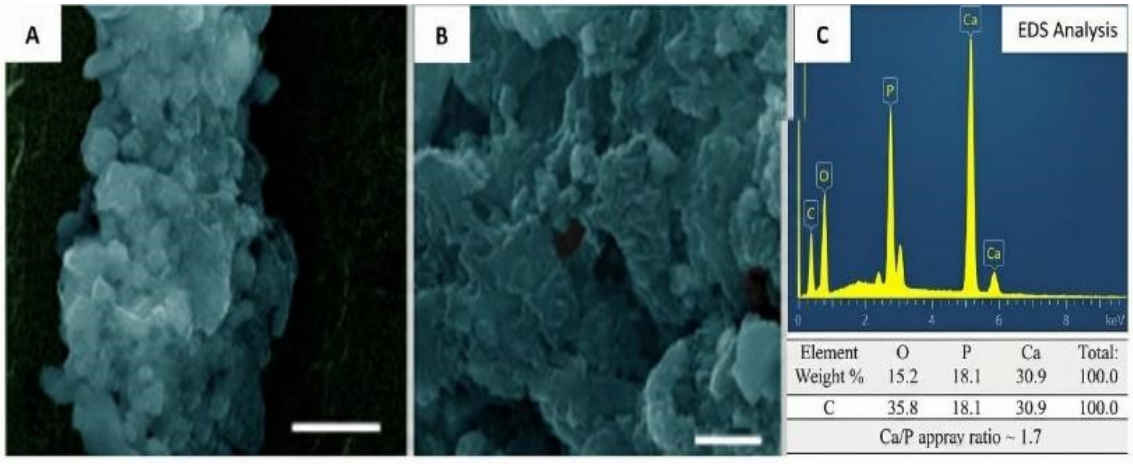

Figure 4. Bioactivity of scaffolds evaluated after 30 days of immersion in Simulated Body Fluid (SBF).Figure (A, B) SEM micrographs of the deposition of apatite-like mineral layers onto the scaffold structure at varying magnifications. (C) EDS analysis that proves the presence of Calcium and Phosphorus, which confirms the biomineralization potential of the scaffold.

Mechanical Properties of the Scaffold

The mechanical performance of the scaffolds was evaluated using a uniaxial compression test. The results indicated that the fabricated scaffold exhibited a compressive strength of approximately 11.2 MPa and a Young's modulus of 89.7 MPa (Table 3).

These mechanical properties suggest that the scaffold possesses sufficient structural stability and mechanical support for potential applications in bone tissue engineering.

Table 3. Mechanical properties of scaffolds

Young's modulus (MPa)	Strain (percentage)	Compressive strength (MPa)
89.7±0.18	1.52±0.8	11.2±0.15

DİSCUSSİON

The aim of tissue engineering approaches is to design scaffolds with structures and biological activities similar to those of the native extracellular matrix (ECM), as well as cellular activities conducive to tissue regeneration. Recently, with the development of various three-dimensional printing techniques, the ability to design scaffolds with controlled structures and geometries has greatly improved. These capabilities are of significant importance for bone tissue engineering, where the porosity, interconnectivity, and surface characteristics of scaffolds are essential for facilitating cell infiltration, nutrient transfer, and tissue formation.

The results of the current study show that the proposed fabrication method is capable of producing scaffolds that create a conducive microenvironment for bone regeneration by integrating various biological cues. The incorporation of these cues within a structurally controlled scaffold matrix provides both mechanical and biological stimulation, which is crucial for effective tissue regeneration. The fabricated scaffolds exhibited an average pore size of 879 ± 12 μm and a porosity of approximately 85%, which exceeds the commonly recommended threshold of 200–350 μm for cancellous bone mimicry [46]. While pore sizes in this range may reduce mechanical resistance, they are associated with enhanced vascularization and nutrient diffusion, which are critical for osteogenesis in larger defect scenarios [46]. These structural characteristics align with findings by Liu et al., who demonstrated that interconnected scaffolds with pore sizes around 500 μm exhibited optimal osteogenic differentiation of human bone marrow-derived mesenchymal stem cells in vitro [47].

Although direct measurements of protein adsorption and degradation behavior were not conducted in this study, some preliminary insights can be inferred from the physicochemical properties of the scaffolds. For instance, the high swelling ratio observed suggests an enhanced ability to absorb fluids, which may support the transport of nutrients, oxygen, and protein molecules within the scaffold. This behavior is consistent with the hydrophilic nature of chitosan and has been reported in comparable composite scaffolds; for example, Phatchayawat et al. observed similarly high swelling in bacterial nanocellulose–chitosan–HAp constructs and attributed it to the hydrophilic character of the polysaccharide matrix [47].

Furthermore, the rough surface morphology identified through characterization is advantageous for scaffold-based bone regeneration. Increased surface roughness can promote protein adsorption from the surrounding environment, thereby enhancing cell adhesion, proliferation, and spreading on the scaffold surface. The enhanced cell viability observed at 24 and 72 h using the CCK-8 assay is consistent with findings from comparable chitosan/HAp scaffolds evaluated with MC3T3-E1 cells. Kabirkoohian et al. similarly reported good cytocompatibility and progressive cell proliferation on hydroxyapatite-coated chitosan scaffolds, attributing this effect to the provision of adequate adhesion sites by the mineral phase . In the present study, the incorporation of Mg into the HAp lattice likely contributes further to this osteogenic environment, as magnesium ions are known to enhance osteoblast proliferation, suppress osteoclast differentiation, and stimulate angiogenesis [45].

In addition, the scaffolds demonstrated good mechanical integrity after 30 days in simulated body fluid (SBF), indicating that their degradation behavior is suitably controlled for bone healing applications. Maintaining structural stability during the early stages of implantation is critical, as the scaffold must provide temporary mechanical support while newly formed bone tissue gradually replaces it. Therefore, the observed stability in SBF suggests that the degradation rate of the scaffold is likely compatible with the initial stages of bone regeneration.

The compressive strength (11.2 MPa) and Young's modulus (89.7 MPa) recorded for the fabricated scaffolds are within a biologically relevant range for bone tissue engineering applications. According to Nazarian et al., human trabecular bone typically exhibits compressive strength in the range of 0.1–30 MPa and modulus values between 10 and 3,000 MPa depending on anatomical site, porosity, and apparent density [38]. The mechanical values obtained in this study fall within the lower range reported for cancellous bone, which is consistent with the high porosity (~85%) of the fabricated scaffolds. Furthermore, these results are comparable to previously reported chitosan/hydroxyapatite-based 3D-printed scaffolds: for example, Ressler et al. reported compressive strength values between 4.04 and 10.17 MPa for UV-crosslinked chitosan/HAp composites [39], while pure porous HA ceramic scaffolds have demonstrated maximum compressive strengths as low as 1.92 MPa [40]. These comparisons confirm that the integration of Mg-HAp within a chitosan matrix via extrusion-based 3D printing yields mechanically superior constructs suitable for non-load-bearing bone defect applications, though further optimization may be required to meet the higher mechanical demands of cortical bone. The antibacterial evaluation performed against Staphylococcus aureus adds an important functional dimension to this study. Implant-associated bacterial infections are among the primary causes of failure in bone grafting and scaffold-based therapies, and the development of scaffolds with intrinsic antibacterial properties is therefore a clinically relevant objective [41].

Chitosan itself is well established as an inherently antibacterial biopolymer, acting primarily through electrostatic disruption of bacterial cell membranes [41]. The bioactive molecules incorporated into the scaffold—particularly naringin and icariin, which have reported anti-inflammatory and antimicrobial properties [29,31] may further contribute to the observed inhibitory effect

against S. aureus. Accordingly, the antibacterial findings of this study are directly relevant to the primary objective of scaffold-supported bone regeneration, as an infection-resistant scaffold can provide a more favorable microenvironment for osteogenesis and reduce post-implantation complications.

The gene expression data from RT-qPCR analysis demonstrated significant upregulation of Wnt and β-catenin markers in MC3T3-E1 cells cultured on the scaffolds, suggesting activation of the Wnt/β-catenin osteogenic signaling pathway. The Wnt/β-catenin pathway is a well-established regulator of osteoblast differentiation and bone formation, and its activation has been extensively documented in osteogenic contexts [42,43]. It should be noted, however, that the conclusions drawn in this study are based solely on mRNA-level data. As highlighted by Cai et al. [44] and Tian et al. [45], mechanistic confirmation of Wnt/β-catenin pathway activation in osteogenic studies typically involves concurrent protein-level analyses—such as western blotting for β-catenin and downstream targets including GSK-3β and Runx2—as well as immunofluorescence imaging to confirm nuclear translocation of β-catenin. Future studies should consider incorporating such analyses to provide a more comprehensive mechanistic understanding of the osteogenic activity of the developed scaffold. However, further studies are required to achieve a more comprehensive understanding of the biological performance of the scaffold system, including long-term degradation behavior and protein adsorption characteristics, for its effective application in bone tissue engineering.

CONCLUSİON

Bioengineered scaffolds fabricated through advanced 3D printing technologies represent a promising strategy for the development of precision regenerative therapies. In this study, a printable chitosan–magnesium-doped hydroxyapatite (Mg-HAp) composite scaffold functionalized with bioactive molecules icariin, lithium chloride, and naringin was successfully developed and characterized under in vitro conditions.

The incorporation of Mg-HAp and bioactive agents resulted in a highly porous scaffold structure with an increased average pore size, which is favorable for cell infiltration and tissue regeneration. In vitro biological evaluations demonstrated enhanced cell viability after 24 and 72 h of culture, indicating good cytocompatibility of the scaffold. Additionally, the scaffold exhibited antibacterial activity against Staphylococcus aureus , a finding of direct clinical relevance, as bacterial infection remains one of the leading causes of bone graft failure and implant-associated complications [41]. The scaffold also significantly upregulated the expression of osteogenic signaling markers associated with the Wnt/β-catenin pathway in MC3T3-E1 cells, as assessed by RT-qPCR gene expression analysis [42,43]. It should be noted that these findings are based on mRNA-level data; future studies incorporating protein-level confirmation such as western blotting for β-catenin and GSK-3β would further substantiate the osteogenic conclusions drawn in this in vitro study [44,45].

The results further indicated that scaffolds containing magnesium-doped hydroxyapatite and bioactive molecules promoted osteogenic gene expression more effectively than the control group under in vitro conditions. Overall, the

developed 3D-printed scaffolds demonstrated favorable cellular compatibility and showed the ability to upregulate osteogenic differentiation markers in vitro. While these characteristics suggest potential applicability in bone tissue regeneration, it should be emphasized that translation of these findings to clinical settings will require rigorous in vivo validation and long-term safety assessment.

To our knowledge, this study is among the first to report the in vitro osteogenic potential of 3D-printed chitosan/Mg-HAp scaffolds simultaneously functionalized with icariin, lithium chloride, and naringin as a combined bioactive system. Within the scope of this in vitro investigation, the incorporation of these bioactive molecules did not adversely affect the physicochemical properties of the scaffolds and showed no evidence of cytotoxicity toward MC3T3-E1 cells.

Future investigations should focus on elucidating the detailed cellular and molecular mechanisms underlying the osteogenic activity of these scaffolds, including protein-level validation of Wnt/β-catenin pathway activation through western blotting or immunofluorescence assays [44,45]. Furthermore, comprehensive in vivo studies will be necessary to fully evaluate their bone healing capacity and long-term performance under physiological conditions, as the present findings are limited to in vitro observations and should be interpreted accordingly.

REFERENCES

1. Bashiri Z, Khosrowpour Z, Moghaddaszadeh A, Jafari D, Alizadeh S, Nasiri H, et al. Optimizations of Placenta Extracellular Matrix-Loaded Silk Fibroin/Alginate 3D-Printed Scaffolds Structurally and Functionally for BoneTissue Engineering. Engineering in Life Sciences. 2025;25(1):e202400085.

2. Utami SS, Raja N, Kim J, Sutejo IA, Park H, Sung A, et al. Support-less 3D bioceramic/extracellular matrix printing in sanitizer-based hydrogel for bone tissueengineering. Biofabrication. 2025;17(2):025017.

3. Mangani S, Vetoulas M, Mineschou K, Spanopoulos K, Vivanco Md,Piperigkou Z, Karamanos NK. Design and applications of extracellular matrix scaffolds in tissue engineering and regeneration. Cells. 2025;14(14):1076.

4. Saghebasl S, Akbarzadeh A, Gorabi AM, Nikzamir N, SeyedSadjadi M,Mostafavi E. Biodegradable functional macromolecules as promising scaffolds for cardiac tissue engineering. Polymers for Advanced Technologies. 2022;33(7):2044-68.

5. Same S, Kadkhoda J, Navidi G, Abedi F, Aghazadeh M, Milani M, et al. The fabrication of halloysite nanotube-based multicomponent hydrogel scaffolds for bone healing. Journal of Applied Biomaterials & Functional Materials.2022;20:22808000221111875.

6. Sagart A, Jahandideh A, Asghari A, Akbarzadeh A, Mortazavi P.Investigating the regenerative effects of PRP and polycaprolactone-hydroxyapatite zeolite nanocomposites on wound healing after tooth extraction. Journal of Comparative Pathobiology. 2022;19(2):3873-82.

7. Rad F, Davaran S, Babazadeh M, Akbarzadeh A, Pazoki-Toroudi H. Biodegradable Electrospun Polyester-Urethane Nanofiber Scaffold: Codelivery Investigation of Doxorubicin-Ezetimibe and Its Synergistic Effect on ProstateCancer Cell Line. Journal of Nanomaterials. 2022;2022(1):8818139.

8. Javadian N, Veshkini A, Jahandideh A, Akbarzadeh A, Asghari A.Ultrasonographic evaluation of Effect of Zeolite and Zeolite/Collagen nanocomposite scaffolds on healing of femur bone defect in rabbits. Veterinary Research & Biological Products. 2021;34(3):114-20.
9. Same S, Navidi G, Samee G, Abedi F, Aghazadeh M, Milani M, et al. Gentamycin-loaded halloysitebased hydrogel nanocomposites for bone tissue-regeneration: fabrication, evaluation of the antibacterial activity and cell response. Biomedical Materials. 2022;17(6):065018.
10. Frumento D, Țălu Ș. Immunomodulatory Potential and Biocompatibility of Chitosan–Hydroxyapatite Bio-composites for Tissue Engineering. Journal of Composites Science. 2025;9(6):305.
11. Shanmugavadivu A, Selvamurugan N. Surface engineering of 3D-printed polylactic acid scaffolds with polydopamine and 4-methoxycinnamic acid–chitosan nanoparticles for bone regeneration. Nanoscale Advances. 2025;7(6):1636-49.
12. Wang X, Yu T, Chen G, Zou J, Li J, Yan J. Preparation and characterization of a chitosan/gelatin/extracellular matrix scaffold and its application in tissue engineering. Tissue Engineering Part C: Methods. 2017;23(3):169-79.
13. Etminanrezaeieh S, Rezazadeh K, Jalilnejad E, Rafiee R. Preparation and characterization of bio-waste derived chitosan/hydroxyapatite/pectin green biocomposite. Scientific Reports. 2025;15(1):24450.
14. Utami R, Habani MH, Sunaryono S, Munasir M, Sani NS, Yustanti E, et al.Natural-Based Magnetite/Hydroxyapatite/Chitosan Nanocomposite as EffectiveDrug Delivery Systems. Journal of Cluster Science. 2025;36(4):143.
15. Di Stefano A, Di Marco C, Toia F, Trapani M, Testa M, Di Leonardo S, et al. Effect of nanocomposite chitosan/hydroxyapatite pH-induced hydrogels on the osteogenic differentiation of spheroids from adipose stem cells. International Journal of Biological Macromolecules. 2025;299:140213.
16. Vidotti R, Yoshikawa A, Sant'Ana M, Souza H, Possebon L, da Rocha DN, et al. Reduction of inflammation and improvement of skin tissue repair using biomaterials composed of hydroxyapatite and chitosan associated to conditioned media derived from dental pulp stem cells. International Journal of Biological Macromolecules. 2025;308:142353.
17. Vaikundam M, Santhanam A. Magnesium oxide nanoparticles incorporated with dual polymers and pectin stabilized hydroxyapatite as a nanocomposite membrane for tissue engineering. Colloids and Surfaces A: Physicochemical and Engineering Aspects. 2025:137963.
18. Liu W, Cheong N, He Z, Zhang T. Application of hydroxyapatite composites in bone tissue engineering: a review. Journal of Functional Biomaterials.2025;16(4):127.
19. Park J-E, Jang Y-S, Bae T-S, Lee M-H. Biocompatibility characteristics of titanium coated with multi walled carbon nanotubes—hydroxyapatite nanocomposites. Materials. 2019;12(2):224.
20. Vaiani L, Boccaccio A, Uva AE, Palumbo G, Piccininni A, Guglielmi P, et al. Ceramic materials for biomedical applications: an overview on properties and fabrication processes. Journal of Functional Biomaterials. 2023;14(3):146.
21. Imtiaz H, Riaz M, Anees E, Bashir F, Hussain T. Biodegradable zinc–magnesium

alloys for bone fixation: A study of their structural integrity,corrosion resistance, and mechanical properties. Materials Chemistry and Physics. 2025;334:130429.

22. Chaudhari YS, Chaudhari MY, Gholap A, Alam MI, Khalid M, Webster TJ, et al. Surface engineering of nano magnesium alloys for orthopedic implants: a systematic review of strategies to mitigate corrosion and promote bone regeneration. Frontiers in Bioengineering and Biotechnology. 2025;13:1617585.

23. Chen M, Cui Y, Li H, Luan J, Zhou X, Han J. Icariin Promotes the Osteogenic Action of BMP2 by Activating the cAMP Signaling Pathway. Molecules. 2019;24:3875.

24. Zhang X-y, Li H-n, Chen F, Chen Y-p, Chai Y, Liao J-z, et al. Icariin regulates miR-23a-3p-mediated osteogenic differentiation of BMSCs via BMP-2/Smad5/Runx2 and WNT/β-catenin pathways in osteonecrosis of the femoral head.Saudi pharmaceutical journal. 2021;29(12):1405-15.

25. Chen H, Weng Z, Kalinowska M, Xiong L, Wang L, Song H, et al. Anti-osteoporosis effect of bioactives in edible medicinal plants: a comprehensive review.Critical Reviews in Food Science and Nutrition. 2025;65(22):4310-26.

26. Vijaykumar A, Mina M. Lithium Chloride Exerts Differential Effects on Dentinogenesis and Osteogenesis in Primary Pulp Cultures. Frontiers in Dental Medicine. 2021;Volume 2 - 2021.

27. Lu C, Chen C, Xu Y, Dai D, Sun C, Li Q. Activation of Wnt/β-cateninsignaling to increase B lymphoma Moloney murine leukemia virus insertion region 1 by lithium chloride attenuates the toxicity of cisplatin in the HEI-OC1 auditory cells. Toxicology Letters. 2025;403:50-65.

28. Yang L, Lyu Z, Fan X, Zheng X, Wang Y. Lithium-Functionalized Sulfonated Polyetheretherketone with Dual Osteogenic-Angiogenic Property: A One-Step Bioactivation Strategy for Enhanced Implants Osseointegration. Advanced Healthcare Materials. 2025:e02072.

29. Xu Y, He P, He B, Chen Z. Bioactive flavonoids metabolites in citrus species: their potential health benefits and medical potentials. Frontiers in Pharmacology. 2025;Volume 16 - 2025.

30. Wilcox L, Borradaile N, Huff M. Antiatherogenic Properties of Naringenin, a Citrus Flavonoid. Cardiovascular Drug Reviews. 2006;17:160-78.

31. Chen T, Li G, Xu Y, Chen B. Naringin Mitigates Chondrocyte Apoptosis in Osteoarthritis by Suppressing the miR-29a-3p-Bax Pathway. Journal of Biochemical and Molecular Toxicology. 2025;39(5):e70304.

32. Lyu T, Liu X, Liu Y, Yang Z, Li P, Lu Y, et al. Naringin in repairing articular cartilage injury by activating TGF-β/Smad signaling pathway to attenuateinflammatory response. Archives of Biochemistry and Biophysics.2025;768:110396.

33. Damiri F, Fatimi A, Liu Y, Musuc AM, Fajardo AR, Gowda BJ, et al.Recent advances in 3D bioprinted polysaccharide hydrogels for biomedicalapplications: A comprehensive review. Carbohydrate polymers. 2025;348:122845.

34. Zhang L, Yang G, Johnson BN, Jia X. Three-dimensional (3D) printed scaffold and material selection for bone repair. Acta biomaterialia. 2019;84:16-33.

35. Hosseini SA, Pourdel B, Rajabi E, Alizadeh A. Surgical Time-Outs: Ritual or Real Safety Practice? Perioperative Care and Operating Room Management.2025:100573.

36. Hefzollesan S. Effect of Scaffolds Containing Chitosan and Hydroxyapatite in Bone Tissue Engineering Using Freeze-Drying Method: A Systematic

Review.Azerbaijan Pharmaceutical and Pharmacotherapy Journal. 2025;24(4):110.

37. Development of extrusion-based 3D-printed chitosan/magnesium-doped nanohydroxyapatite scaffolds functionalized with icariin, lithium chloride and naringin for enhanced bone regeneration in vitro and in vivo, Sahar Hefzollesan a,b , Hanife Musayeva a, Hamed Aghazadeh a,c ,d,h , Aslan Mammadov a, Soheila Ajdary e, Rauf Baylarov f, Sahra Hefzollesan g, Rizvan Mammadov a,https://doi.org/10.1016/j.ijbiomac.2026.151005

38. Nazarian A, von Stechow D, Zurakowski D, Muller R, Snyder BD. Bone volume fraction explains the variation in strength and stiffness of cancellous bone affected by metastatic cancer and osteoporosis. Calcif Tissue Int. 2008;83(6):368-79. doi:10.1007/s00223-008-9174-x

39. Ressler A, Antunovic M, Teruel-Biosca L, Ferrer GG, Urlić I, Ivanković M, et al. Bioresorbable Chitosan-Based Bone Regeneration Scaffold Using Various Bioceramics and the Alteration of Photoinitiator Concentration in an Extended UV Photocrosslinking Reaction. Gels. 2022;8(11):696. doi:10.3390/gels8110696

40. Wei Q, Wang Y, Chai W, Zhang Y, Chen X. Molecular dynamics simulation and experimental study of the bonding characteristics of polymer binders in 3D powder printed hydroxyapatite bioceramic bone scaffolds. Ceram Int. 2022;48(24):36887-96. doi:10.1016/j.ceramint.2022.08.240

41. Tian Y, Wu D, Wu D, Cui Y, Ren G, Wang Y, et al. Chitosan-Based Biomaterial Scaffolds for the Repair of Infected Bone Defects. Front Bioeng Biotechnol. 2022;10:899760. doi:10.3389/fbioe.2022.899760

42. Arya PN, Saranya I, Selvamurugan N. Crosstalk between Wnt and bone morphogenetic protein signaling during osteogenic differentiation. World J Stem Cells. 2024;16(2):102-113. doi:10.4252/wjsc.v16.i2.102

43. Cai Y, Sun H, Song X, Zhao J, Xu D, Liu M. The Wnt/β-catenin signaling pathway inhibits osteoporosis by regulating the expression of TERT: an in vivo and in vitro study. Aging (Albany NY). 2023;15(19):10326-10344. doi:10.18632/aging.205136

44. Abbasi N, Hamlet S, Love RM, Nguyen NT. Porous scaffolds for bone regeneration. J Sci Adv Mater Dev. 2020;5(1):1-9. doi:10.1016/j.jsamd.2020.01.007

45. Liu W, Cheong N, He Z, Zhang T. Application of hydroxyapatite composites in bone tissue engineering: a review. J Funct Biomater. 2025;16(4):127. doi:10.3390/jfb16040127

46. Phatchayawat P, Boonkum W, Chaikittiratana A, Puttiwong N, Chaivisuthangkura A. Bacterial Nanocellulose–Chitosan–Gelatin–Hydroxyapatite Scaffolds for Bone Tissue Engineering. Macromol Biosci. 2025;25:e202500299. doi:10.1002/mabi.202500299

47. Kabirkoohian A, Bakhshi H, Irani S, Sharifi F. Hydroxyapatite-coated carboxymethyl chitosan scaffolds for promoting osteoblast and stem cell differentiation. Appl Biochem Biotechnol. 2023;195(6):3888-3899. doi:10.1007/s12010-022-03916-6

SÜMÜK REGENERASİYASININ GÜCLƏNDİRİLMƏSİ ÜÇÜN BİOAKTİV MOLEKULLARLA YÜKLƏNMİŞ 3D ÇAP EDİLMİŞ XİTOZAN/MAQNEZİUM DOPİNQLİ HİDROKSİAPATİT SKAFOLDLARININ BİOLOJİ QİYMƏTLƏNDİRİLMƏSİ

Hefzollesan Sahar [12], Məmmədov A.[1], Musayeva H.[1], Hefzollesan Sahra [3], Məmmədov R.[1]*

[1] Azərbaycan Tibb Universiteti, terapevtik stomatologiya və ortopedik stomatologiya kafedrası, Bakı, Azərbaycan

[2] MedEra Xəstəxanası, Stomatologiya şöbəsi, Bakı, Azərbaycan

[3] Qaradəniz Texniki Universiteti, Stomatologiya fakültəsi, Trabzon, Türkiyə

**E-mail: sahar.hefzollesan@amu.edu.az*

Xülasə

Osteogenezi stimullaşdıra bilən bioaktiv skafoldların hazırlanması sümük toxuması mühəndisliyində əsas problemlərdən biridir. Bu tədqiqatda ikarin, litium xlorid və naringin ilə funksionallaşdırılmış xitozan və maqnezium dopinqli hidroksiapatitdən (Mg-HAp) ibarət bioaktiv nanokompozit skafoldun bioloji xüsusiyyətləri araşdırılmışdır. Skafold ekstrüziya əsaslı 3D çap texnologiyası ilə hazırlanmış və onun xüsusiyyətləri **in vitro** və **in vivo** bioloji testlər vasitəsilə qiymətləndirilmişdir. Hüceyrə yapışması, proliferasiyası və osteogen siqnal aktivliyi osteoblastabənzər MC3T3-E1 hüceyrələri vasitəsilə qiymətləndirilmişdir. Hüceyrə canlılığı CCK-8 testi ilə müəyyən edilmiş, Wnt və β-katenin siqnal markerlərinin gen ifadəsi isə Real-Time PCR üsulu ilə analiz edilmişdir. Antimikrob aktivlik *Staphylococcus aureus* bakteriyasına qarşı minimum inhibitor konsentrasiyası (MIC) metodu ilə qiymətləndirilmişdir. Bundan əlavə, sümük regenerasiyası potensialı siçovul kəllə sümüyündə yaradılmış defekt modeli üzərində histoloji analiz vasitəsilə araşdırılmışdır.

Nəticələr göstərmişdir ki, skafold səthində hüceyrə proliferasiyası nəzarət qrupu ilə müqayisədə əhəmiyyətli dərəcədə artmışdır. Gen ifadəsi analizləri Wnt/β-katenin siqnal yolunun aktivləşdiyini göstərmişdir ki, bu da osteogen mexanizmlərin stimullaşdırıldığını göstərir. Skafold həmçinin 512 μg/ml MIC dəyəri ilə antibakterial aktivlik nümayiş etdirmişdir. Histoloji qiymətləndirmə 8 və 12 həftədən sonra implantasiya olunmuş skafold ətrafında yeni sümük formalaşması və kollagen depozisiyasının tədricən artdığını təsdiq etmişdir. Bu nəticələr göstərir ki, bioaktiv molekullarla yüklənmiş xitozan/Mg-HAp skafoldları yüksək osteogen potensiala malikdir və sümük toxuması mühəndisliyi sahəsində perspektivli material hesab oluna bilər.

БИОЛОГИЧЕСКАЯ ОЦЕНКА 3D-НАПЕЧАТАННЫХ КАРКАСОВ ИЗ ХИТОЗАНА/ГИДРОКСИАПАТИТА, ЛЕГИРОВАННОГО МАГНИЕМ, ЗАГРУЖЕННЫХ БИОАКТИВНЫМИ МОЛЕКУЛАМИ, ДЛЯ УСИЛЕННОЙ РЕГЕНЕРАЦИИ КОСТНОЙ ТКАНИ

Хефзоллесан Сахар[12], Мамедов А.[1], Мусаева Х.[1], Хефзоллесан Сахра[3], Мамедов Р.[1]*

[1] Кафедра терапевтической стоматологии и ортопедической стоматологии, Азербайджанский медицинский университет, Баку, Азербайджан

[2] Больница MedEra, Стоматологическое отделение, Баку, Азербайджан

[3] Караденизский технический университет, факультет стоматологии, Трабзон, Турция

**E-mail: sahar.hefzollesan@amu.edu.az*

Резюме

Разработка биоактивных каркасов, способных стимулировать остеогенез, является одной из ключевых задач в области инженерии костной ткани. В настоящем исследовании была изучена биологическая эффективность биоактивного нанокомпозитного каркаса, состоящего из

хитозана и гидроксиапатита, легированного магнием (Mg-HAp), функционализированного икарином, хлоридом лития и нарингином. Каркас был изготовлен с использованием технологии экструзионной 3D-печати и оценен с помощью **in vitro** и **in vivo** биологических тестов. Остеобластоподобные клетки MC3T3-E1 использовались для оценки адгезии клеток, их пролиферации и активности остеогенных сигнальных путей. Жизнеспособность клеток определяли с помощью теста CCK-8, а экспрессию генов сигнальных маркеров Wnt и β-катенина анализировали методом Real-Time PCR. Антимикробная активность против *Staphylococcus aureus* оценивалась методом определения минимальной ингибирующей концентрации (MIC). Кроме того, потенциал регенерации костной ткани исследовали на модели дефекта теменной кости крыс с последующим гистологическим анализом.

Результаты показали значительное увеличение пролиферации клеток на поверхности каркаса по сравнению с контрольной группой. Анализ экспрессии генов выявил активацию сигнального пути Wnt/β-катенина, что свидетельствует о стимулировании остеогенных механизмов. Каркас также проявил антибактериальную активность с MICзначением 512 мкг/мл. Гистологическое исследование подтвердило прогрессирующее образование новой костной ткани и отложение коллагена вокруг имплантированного каркаса через 8 и 12 недель. Полученные результаты свидетельствуют о том, что каркасы из хитозана/Mg-HAp, загруженные биоактивными молекулами, обладают высоким остеогенным потенциалом и могут рассматриваться как перспективные материалы для применения в инженерии костной ткани.